CMS Technical Summary Report #89-28

ANALYSIS OF SPURT PHENOMENA FOR A NON-NEWTONIAN FLUID

David S. Malkus, John A. Nohel
and Bradley J. Plohr

UNIVERSITY OF WISCONSIN

CENTER FOR THE MATHEMATICAL SCIENCES

Center for the Mathematical Sciences
University of Wisconsin—Madison
610 Walnut Street
Madison, Wisconsin 53705

March 1989

(Received March 30, 1989)

Sponsored by

U.S. Army Research Office
P. O. Box 12211
Research Triangle Park,
North Carolina 27709

National Science
Foundation
Washington, DC 20550

Air Force Office of
Scientific Research
Washington, DC 20332

UNIVERSITY OF WISCONSIN-MADISON
CENTER FOR THE MATHEMATICAL SCIENCES

ANALYSIS OF SPURT PHENOMENA FOR A NON-NEWTONIAN FLUID *

David S. Malkus [1]
John A. Nohel [2]
Bradley J. Plohr [3]

CMS Technical Summary Report #89-28
March 1989

Abstract

We discuss novel phenomena in dynamic shearing flows of non-Newtonian fluids of importance for polymer processing. A striking example is "spurt" which was observed experimentally in the flow of monodispersive polyisoprenes through capillaries; the volumetric flow rate increased dramatically at a critical stress independent of molecular weight. We show that satisfactory explanation of spurt requires studying the full dynamics of the equations of motion and constitutive relations characterized by a non-monotonic relation between the steady shear stress and strain rate. The increase in volumetric flow rate is shown to correspond to jumps in the strain rate when the driving pressure gradient exceeds a critical value. Motivated by scaling suggested by accurate numerical computations of the governing dynamic problem that yielded qualitative and quantitative agreement with experiment, we introduce a system of ordinary differential equations that approximates dynamic behavior of highly elastic and very viscous fluids. The complete dynamics of the system of ode's is determined by phase plane analysis. These results are then used to explain not only spurt but also shape memory, hysteresis, latency, and other effects that have also been observed in numerical simulations.

AMS (MOS) Subject Classifications: 34C15, 34C35, 34D20, 34E99, 35K55, 35L60, 35L65, 35L67, 65M99, 73F15, 76A05, 76A10

Key Words: change of type, hysteresis, invariant region, latency, Lyapunov function, non-Newtonian, periodic solution, phase plane analysis, shape memory, shear flow, spurt

* Supported by the U. S. Army Research Office under Grant DAAL03-87-K-0036, the National Science Foundation under Grants DMS-8712058 and DMS-8620303, and the Air Force Office of Scientific Research under Grants AFOSR-87-0191 and AFOSR-85-0141.

[1] Also Department of Engineering Mechanics.

[2] Also Department of Mathematics.

[3] Also Computer Sciences Department.

1. Introduction

The purpose of this paper is to analyze novel phenomena in dynamic shearing flows of non-Newtonian fluids that are important for polymer processing. Understanding such behavior has proved to be of significant physical, mathematical, and computational interest. One striking phenomenon, called "spurt," was observed by Vinogradov *et al.* [20] in the flow of monodispersive polyisoprenes through capillaries. They found that the volumetric flow rate increased dramatically at a critical stress that was independent of molecular weight. Until recently, spurt had been overlooked or dismissed by rheologists because no plausible mechanism was known to explain it in the context of steady flows that are linearly stable.

We find that satisfactory explanation and modeling of the spurt phenomenon requires studying the full dynamics of the equations of motion and constitutive equations. The common feature of constitutive models that exhibit spurt is a non-monotonic relation between the steady shear stress and strain rate. This allows jumps in the steady strain rate to form when the driving pressure gradient exceeds a critical value; such jumps correspond to the sudden increase in volumetric flow rate observed in the experiments of Vinogradov *et al.* Hunter and Slemrod [7] studied the qualitative behavior of these jumps in a one-dimensional viscoelastic model of rate type and predicted shape memory and hysteresis effects related to spurt. A salient feature of this model is linear instability and loss of evolutionarity in a region of state space. By contrast, the equations that are analyzed in the present work derive from a fully three-dimensional constitutive relation and remain stable and evolutionary, as we would expect of a realistic model. This model also exhibits spurt, shape memory, and hysteresis; furthermore, it predicts other effects, such as latency, normal stress oscillations, and molecular weight dependence of hysteresis, that can be tested in rheological experiment.

In Refs. [9, 12, 13], effective numerical methods were developed for simulating one-dimensional shear flows at high Weissenberg (Deborah) number; calculations using these methods agreed qualitatively and quantitatively with experiment. We discussed preliminary results on global existence and stability of discontinuous steady states, and we introduced a system of ordinary differential equations that approximate the dynamics of highly elastic and very viscous fluids, such as those in the experiments of Vinogradov *et al.* The objective of the present paper is to analyze this approximating dynamical system. Based on this analysis, we explain the shape memory, hysteresis, latency, and other effects that have been observed in the numerical simulations. Similar results are known for related constitutive models: a model with two or more relaxation times and no Newtonian viscosity is analyzed mathematically in Ref. [14]; and another model with a single relaxation time and Newtonian viscosity is studied numerically in Ref. [10]. Therefore we believe that our results are not limited to the specific model that we study.

The paper is organized as follows: Sec. 2 formulates and discusses the flow model; Sec. 3 provides a complete description of the dynamics of the approximating quadratic system of ordinary differential equations by means of a phase plane analysis; Sec. 4 uses the results of Sec. 3 to describe features of the mathematical model in relation to the experiments of Vinogradov *et al.* and explains latency, shape memory, and hysteresis analytically; and Sec. 5 discusses certain physical and mathematical conclusions.

2. The Flow Model

The motion of a fluid under incompressible and isothermal conditions is governed by the balance of mass and linear momentum. The response characteristics of the fluid are embodied in the constitutive relation for the stress. For viscoelastic fluids with fading memory, these relations specify the stress as a functional of the deformation history of the fluid. Many sophisticated constitutive models have been devised; see Ref. [1] for a survey. In the present work, we focus on a particular differential model that is explained in more detail in Ref. [13]. This model can be regarded as a special case of the Johnson-Segalman model [8] and of the Oldroyd constitutive equation [17]. We believe, however, that qualitative aspects of our results are not limited to this particular model; results on similar models [14, 10] confirm this.

Essential properties of constitutive relations are exhibited in simple planar Poiseuille shear flow. We study the Poiseuille shear flow between parallel plates located at $x = \pm h/2$, with the flow aligned along the y-axis (see Fig. 1). Therefore, the flow variables are independent of y, and the velocity field is $\mathbf{v} = (0, v(x,t))$, which implies that the balance of mass is automatically satisfied. The stress is decomposed into three parts: an isotropic pressure p; a Newtonian contribution, characterized by viscosity η; and an extra stress, characterized by a shear modulus μ and a relaxation rate λ. In shear flow, the components of the extra stress tensor Σ can be written $\Sigma^{xx} = Z(x,t)/(1+a)$, $\Sigma^{xy} = \Sigma^{yx} = \sigma(x,t)$, and $\Sigma^{yy} = -Z(x,t)/(1-a)$, while the pressure takes the form $p = p_0(x,t) - f(t)y$, f being the pressure gradient driving the flow. Here $a \in (-1,1)$ is a slip parameter defining the model.

To simplify notation, we nondimensionalize the variables by scaling distance by h, time by λ^{-1}, and stress by μ. Furthermore, if we replace σ, v, and f by $\hat{\sigma} := (1-a^2)^{1/2}\sigma$, $\hat{v} := (1-a^2)^{1/2}v$, and $\hat{f} := (1-a^2)^{1/2}f$, respectively, then the parameter a disappears from the governing equations. Since no confusion will arise, we omit the caret. There are two essential dimensionless parameters:

$$\alpha := \rho h^2 \lambda^2 / \mu \,, \tag{2.1}$$

a ratio of Reynolds number to Deborah number (ρ being the constant density); and

$$\varepsilon := \eta\lambda/\mu \,, \tag{2.2}$$

a ratio of viscosities.

The resulting initial–boundary-value problem governing the flow [13] is the system

$$\begin{aligned} &\alpha v_t - \sigma_x = \varepsilon v_{xx} + f \,, \\ &\sigma_t - (Z+1)v_x = -\sigma \,, \\ &Z_t + \sigma v_x = -Z \end{aligned} \tag{JS}$$

on the interval $[-1/2, 0]$, with boundary conditions

$$v(-1/2,t) = 0 \quad \text{and} \quad v_x(0,t) = 0 \tag{BC}$$

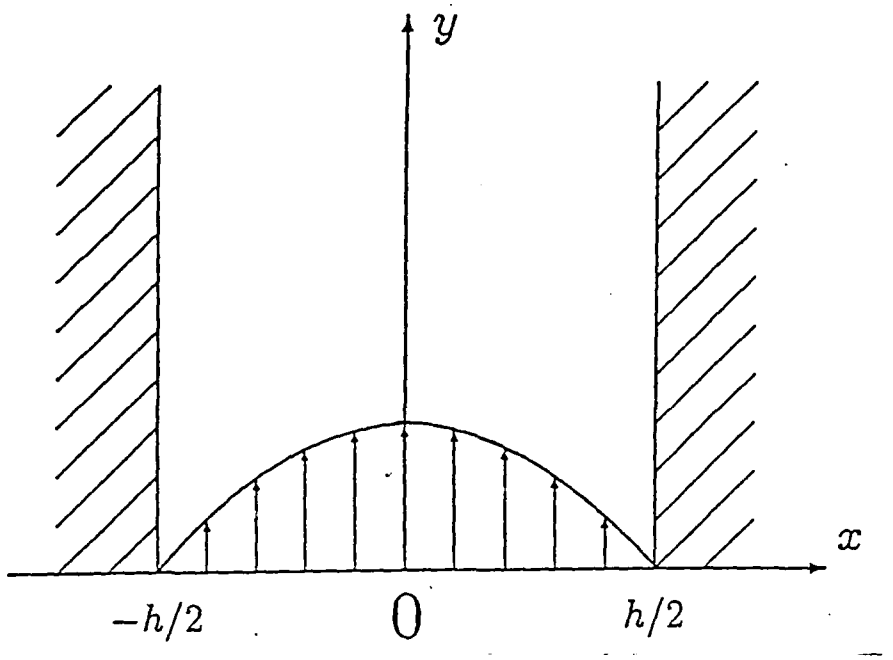

Fig. 1: Shear flow through a slit-die.

and initial conditions

$$v(x,0) = v_0(x)\ , \quad \sigma(x,0) = \sigma_0(x)\ , \quad \text{and} \quad Z(x,0) = Z_0(x)\ , \qquad (IC)$$

where the compatibility conditions $v_0(-1/2) = 0$, $v_0'(0) = 0$ and $\sigma_0(0) = 0$ are assumed to hold.

If $\varepsilon = 0$, the system can be classified according to type: when $Z+1 \geq 0$, the system is hyperbolic, with characteristics speeds 0 and $\pm[(Z+1)/\alpha]^{1/2}$; if $Z+1 < 0$, by contrast, the system has a pair of pure imaginary characteristic speeds, in addition to the speed 0, and (JS) ceases to be evolutionary. This classification, however, is not applicable when $\varepsilon > 0$, which we assume throughout the present work. In the case $\varepsilon > 0$, it was shown recently [6] that the problem (JS), (BV), (IC) possesses a unique classical solution globally in time for smooth initial data of arbitrary size. However, it is has not been proved that the solution tends to a limiting steady state as t tends to infinity.

The steady-state solution of system (JS), when the forcing term f is a constant $\overline{f}$, plays an important role in our discussion. Such a solution, denoted by $\overline{v}$, $\overline{\sigma}$, and $\overline{Z}$, can be described as follows. The stress components $\overline{\sigma}$ and $\overline{Z}$ are related to the strain rate $\overline{v}_x$ through

$$\overline{\sigma} = \frac{\overline{v}_x}{1+\overline{v}_x^2} \qquad (2.3)$$

and

$$\overline{Z} + 1 = \frac{1}{1 + \overline{v}_x^2} \, . \tag{2.4}$$

Therefore, the steady total shear stress $\overline{T} := \overline{\sigma} + \varepsilon \overline{v}_x$ is given by $\overline{T} = w(\overline{v}_x)$, where

$$w(s) := \frac{s}{1 + s^2} + \varepsilon s \, . \tag{2.5}$$

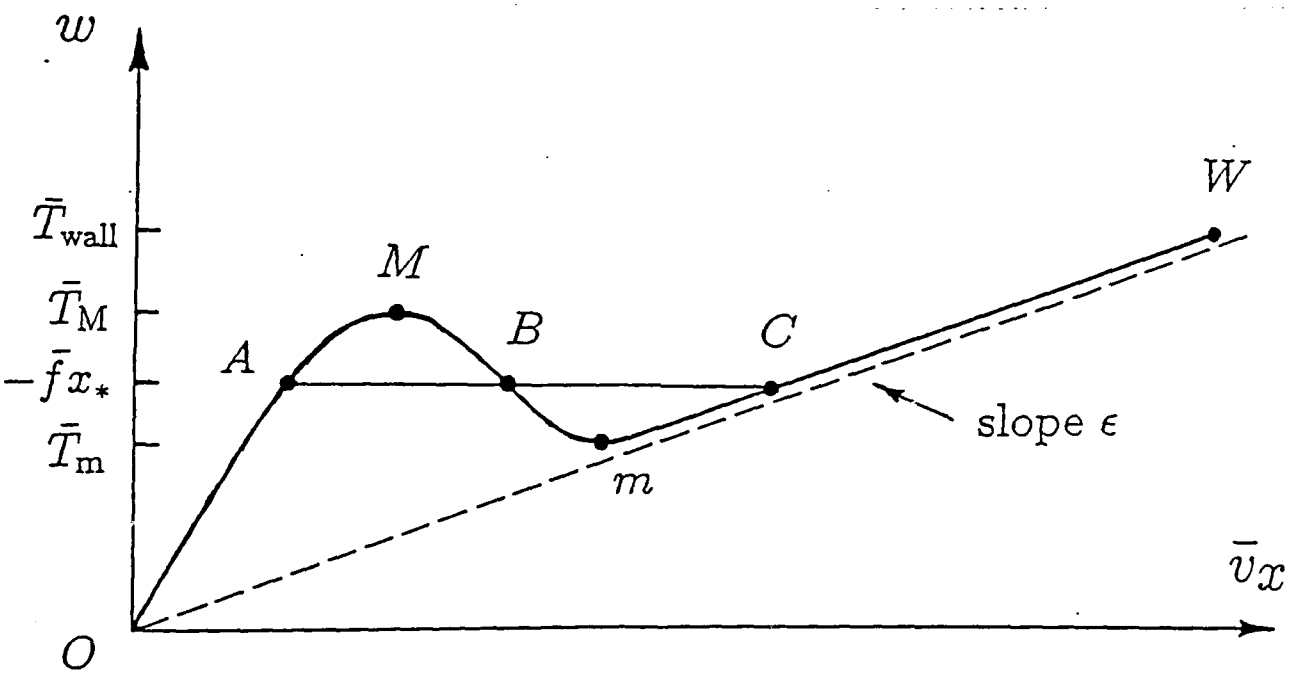

Fig. 2: Total steady shear stress $\overline{T}$ *vs.* shear strain rate $\overline{v}_x$ for steady flow. The case when $\overline{f} > 0$ and there are three critical points is illustrated; other possibilities are discussed in Secs. 3 and 4.

The properties of w, the steady-state relation between shear stress and shear strain rate, are crucial to the behavior of the flow. By symmetry, it suffices to consider non-negative strain rates, $s \geq 0$. For all $\varepsilon > 0$, the function w has inflection points at $s = 0$ and $s = \sqrt{3}$. When $\varepsilon > 1/8$, the function w is strictly increasing, but when $\varepsilon < 1/8$, the function w is not monotone. Lack of monotonicity is the fundamental cause of the non-Newtonian behavior studied in this paper, so hereafter we assume that $\varepsilon < 1/8$.

The graph of w is shown in Fig. 2. Specifically, w has a maximum at $s = s_M$ and a minimum at $s = s_m$, where

$$s_M, s_m = \left[\frac{1 - 2\varepsilon \mp \sqrt{1 - 8\varepsilon}}{2\varepsilon}\right]^{1/2} , \tag{2.6}$$

respectively, at which points it takes the values $\overline{T}_M := w(s_M)$ and $\overline{T}_m := w(s_m)$. As $\varepsilon \to 1/8$, the two critical points coalesce at $s = \sqrt{3}$.

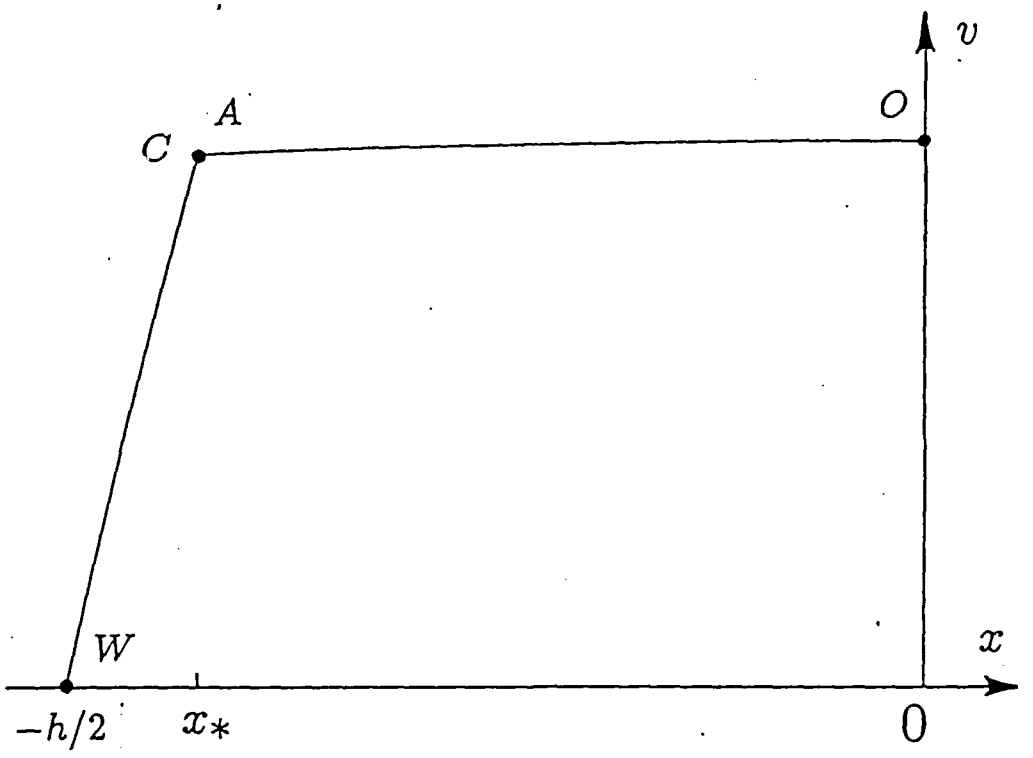

Fig. 3: Velocity profile for steady flow.

The momentum equation, together with the boundary condition at the centerline, implies that the steady total shear stress satisfies $\overline{T} = -\overline{f}x$ for every $x \in [-\frac{1}{2}, 0]$. Therefore, the steady velocity gradient can be determined as a function of x by solving

$$w(\overline{v}_x) = -\overline{f}x \ . \tag{2.7}$$

Equivalently, a steady state solution $\overline{v}_x$ satisfies the cubic equation $P(\overline{v}_x) = 0$, where

$$P(s) := \varepsilon\, s^3 - \overline{T}\, s^2 + (1 + \varepsilon)s - \overline{T} \ . \tag{2.8}$$

The steady velocity profile in Fig. 3 is obtained by integrating $\overline{v}_x$ and using the boundary condition at the wall. However, because the function w is not monotone, there might be up to three distinct values of $\overline{v}_x$ that satisfy Eq. (2.7) for any particular x on the interval $[-1/2, 0]$. Consequently, $\overline{v}_x$ can suffer jump discontinuities, resulting in kinks in the velocity profile (as at the point x_* in Fig. 3). Indeed, a steady solution must contain such a jump if the total stress $\overline{T}_{\text{wall}} = |\overline{f}|/2$ at the wall exceeds the total stress $\overline{T}_M$ at the local maximum M in Fig. 2.

Equation (2.7) implies that the stress $\Sigma := \sigma + \varepsilon v_x + \overline{f}x$ vanishes throughout the channel in steady state. The numerical simulations of (JS) in Ref. [13] suggest that Σ tends to zero as t tends to infinity for every x, even though the limiting solution can suffer discontinuities in $\overline{v}_x$ and $\overline{\sigma}$ whenever $-|\overline{f}|x$ lies between the values $\overline{T}_m$ and $\overline{T}_M$ of w in Fig. 2. Therefore the discontinuities in σ and εv_x seem to cancel. This behavior has been proved recently [16] for a simpler model problem that captures several key features of (JS). It is also shown that the discontinuous steady solution is stable with respect to small perturbations of initial data. Current work of Nohel, Pego, and Tzavaras indicates that a similar stability result holds for solutions of (JS) whenever the parameter α is sufficiently small.

3. Phase Plane Analysis for System (JS) When $\alpha = 0$

A great deal of information about the structure of solutions of system (JS) can be garnered by studying a system of ordinary differential equations that approximates it in a certain parameter range. Motivation for this approximation comes from the following observation: in experiments of Vinogradov *et al.* [20], $\alpha = \rho h^2 \lambda^2/\mu$ is of the order 10^{-12}; thus the term αv_t in the momentum equation of system (JS) is negligible even when v_t is moderately large. We are led to study the approximation to system (JS) obtained when $\alpha = 0$. The behavior of solutions of the resulting dynamical system offers an explanation for several features of the solutions of the full system (JS) observed in the computations of Refs. [9, 13]; in fact, these calculations prompted the following analysis, which determines the dynamics of the approximating system completely.

When $\alpha = 0$, the momentum equation in system (JS) can be integrated, just as in the case of steady flows, to show that the total shear stress $T := \sigma + \varepsilon v_x$ coincides with the steady value $\overline{T}(x) = -\overline{f}x$. Thus $T = \overline{T}(x)$ is a function of x only, even though σ and v_x are functions of both x and t. The remaining equations of system (JS) yield, for each fixed x, the autonomous planar system of ordinary differential equations

$$\begin{aligned} \dot{\sigma} &= (Z+1)\left(\frac{\overline{T}-\sigma}{\varepsilon}\right) - \sigma \,, \\ \dot{Z} &= -\sigma\left(\frac{\overline{T}-\sigma}{\varepsilon}\right) - Z \,. \end{aligned} \tag{3.1}$$

Here the dot denotes the derivative d/dt. We emphasize that a different dynamical system is obtained at each point on the interval $[-1/2, 0]$ in the channel because $\overline{T}$ depends on x. These dynamical systems can be analyzed completely by a phase-plane analysis, which we carry out in some detail.

The critical points of system (3.1) satisfy the algebraic system

$$\begin{aligned} &(Z+1+\varepsilon)\left(\frac{\sigma}{\overline{T}}-1\right)+\varepsilon=0\,, \\ &\frac{\overline{T}^2}{\varepsilon}\frac{\sigma}{\overline{T}}\left(\frac{\sigma}{\overline{T}}-1\right)-Z=0\,. \end{aligned} \tag{3.2}$$

Eliminating Z in these equations shows that the σ-coordinates of the critical points satisfy the cubic equation $Q(\sigma/\overline{T})=0$, where

$$Q(\xi):=\left[\frac{\overline{T}^2}{\varepsilon}\xi(\xi-1)+1+\varepsilon\right](\xi-1)+\varepsilon\,. \tag{3.3}$$

Since

$$P(\overline{v}_x)=P\left(\frac{\overline{T}-\sigma}{\varepsilon}\right)=\frac{\overline{T}}{\varepsilon}Q(\sigma/\overline{T}) \tag{3.4}$$

[*cf.* Eqs. (2.8) and (3.3)], each critical point of the system (3.1) defines a steady-state solution of system (JS): such a solution corresponds to a point on the steady total-stress curve (see Fig. 2) at which the total stress is $\overline{T}(x)$.

By symmetry, we may focus attention on the case $\overline{T}>0$. Consequently, for each position x in the channel and for each $\varepsilon>0$, there are three possibilities:
(1) there is a single critical point A when $\overline{T}<\overline{T}_m$;
(2) there is also a single critical point C if $\overline{T}>\overline{T}_M$;
(3) there are three critical points A, B, and C when $\overline{T}_m<\overline{T}<\overline{T}_M$.
For simplicity, we ignore the degenerate cases, where $\overline{T}=\overline{T}_M$ or $\overline{T}=\overline{T}_m$, in which two critical points coalesce.

To determine the qualitative structure of the dynamical system (3.1), we first study the nature of the critical points. The behavior of orbits near a critical point depends on the linearization of Eq. (3.1) at this point, *i.e.*, on the eigenvalues of the Jacobian

$$\mathbf{J}=\begin{pmatrix} -\frac{1}{\varepsilon}(Z+1+\varepsilon) & -\frac{\overline{T}}{\varepsilon}\left(\frac{\sigma}{\overline{T}}-1\right) \\ \frac{\overline{T}}{\varepsilon}\left(2\frac{\sigma}{\overline{T}}-1\right) & -1 \end{pmatrix}\,, \tag{3.5}$$

evaluated at the critical point. The character of the eigenvalues of J can be determined from the signs of the trace of $\mathbf{J}$, given by

$$-\varepsilon\,\mathrm{Tr}\,\mathbf{J}=Z+1+2\varepsilon\,; \tag{3.6}$$

the determinant of $\mathbf{J}$, given by

$$\varepsilon\,\mathrm{Det}\,\mathbf{J}=Z+1+\varepsilon+\frac{\overline{T}^2}{\varepsilon}\left(2\frac{\sigma}{\overline{T}}-1\right)\left(\frac{\sigma}{\overline{T}}-1\right)\,; \tag{3.7}$$

and the discriminant of **J**, given by

$$\epsilon^2 \,\mathrm{Discrm}\,\mathbf{J} = (Z+1)^2 - 8\overline{T}^2\left(\frac{\sigma}{\overline{T}} - \frac{3}{4}\right)^2 + \tfrac{1}{2}\overline{T}^2 \,. \tag{3.8}$$

We note a useful fact: at a critical point,

$$\epsilon \,\mathrm{Det}\,\mathbf{J} = Q'(\sigma/\overline{T}) \,; \tag{3.9}$$

this follows by using the second of Eqs. (3.2) to replace Z in Eq. (3.7). This relation is important because Q' is positive at A and C and negative at B.

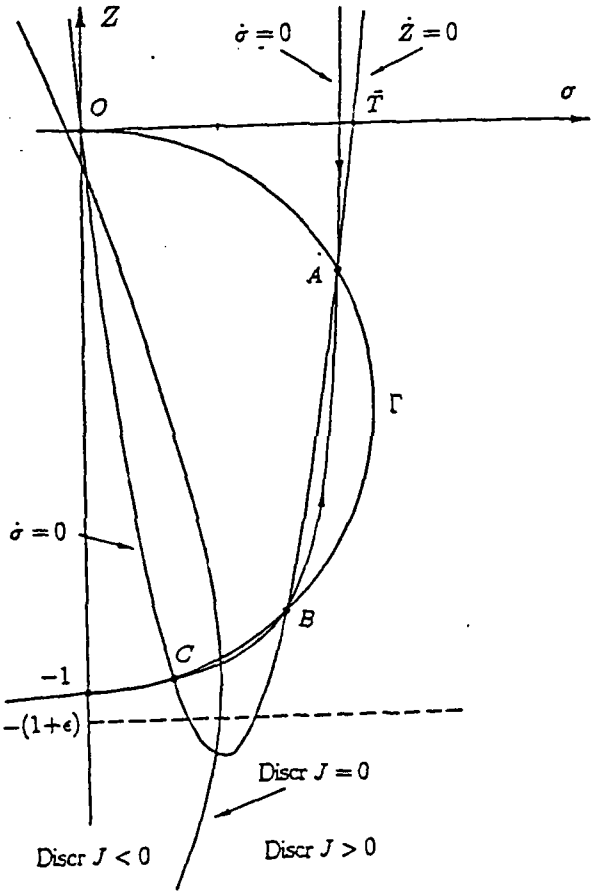

Fig. 4: The phase plane in the case of three critical points.

The character of the eigenvalues can be understood using these formulae together with Fig. 4. In this figure is drawn the hyperbola on which $\dot\sigma = 0$ and parabola on which $\dot Z = 0$ [see Eqs. (3.2)]. These curves intersect at the critical points of the dynamical system for the given choice of ϵ and $\overline{T}$; Fig. 4 corresponds to the most comprehensive case of three critical points. Notice that, having scaled the σ-coordinate by $\overline{T}$, the hyperbola on which $\dot\sigma = 0$ is independent of $\overline{T}$. Also drawn in Fig. 4 is the hyperbola on which Discrm **J** vanishes. We draw the following conclusions:

(1) $\mathrm{Tr}\,\mathbf{J} < 0$ at all critical points;
(2) $\mathrm{Det}\,\mathbf{J} > 0$ at A and C, while $\mathrm{Det}\,\mathbf{J} < 0$ at B; and
(3) $\mathrm{Discrm}\,\mathbf{J} > 0$ at A and B, whereas $\mathrm{Discrm}\,\mathbf{J}$ can be of either sign at C. (For typical values of ε and $\overline{T}$, $\mathrm{Discrm}\,\mathbf{J} < 0$ at C; in particular, $\mathrm{Discrm}\,\mathbf{J} < 0$ if C is the only critical point. But it is possible for $\mathrm{Discrm}\,\mathbf{J}$ to be positive if $\overline{T}$ is sufficiently close to $\overline{T}_m$.)

Standard theory of nonlinear planar dynamical systems (see, *e.g.*, Ref. [2, Chap. 15]) now establishes the local characters of the critical points:

(1) A is an attracting node (called the classical attractor);
(2) B is a saddle point; and
(3) C is either an attracting spiral point or an attracting node (called the spurt attractor).

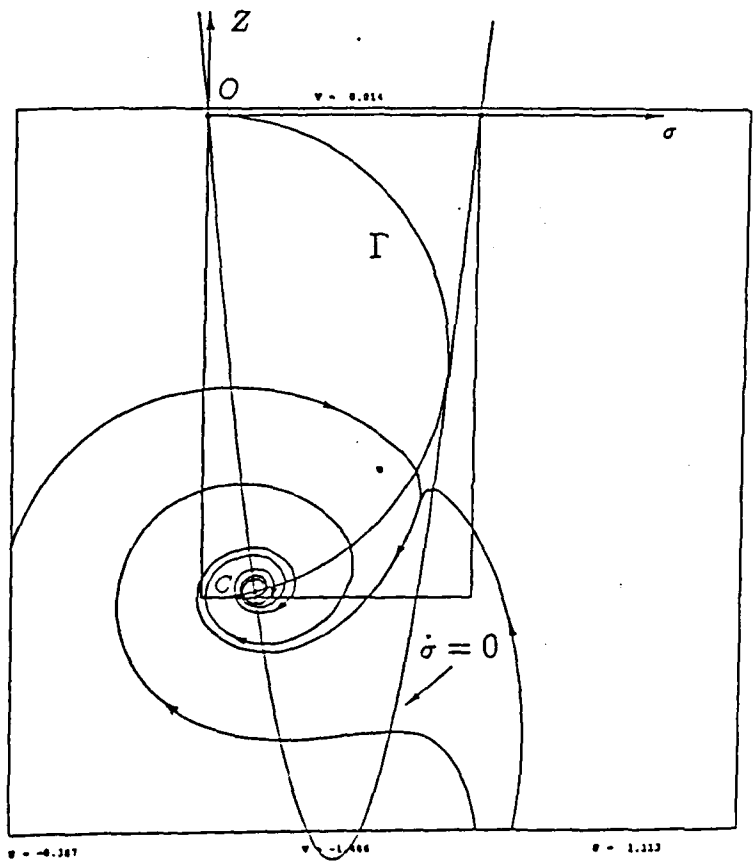

Fig. 5: The phase plane when the spurt attractor C is the only critical point.

To understand the global qualitative behavior of orbits, we construct suitable invariant sets. In this regard, a useful tool is the identity

$$\frac{d}{dt}\left\{\sigma^2 + (Z+1)^2\right\} = -2\left[\sigma^2 + (Z+\tfrac{1}{2})^2 - \tfrac{1}{4}\right] , \tag{3.10}$$

which is obtained by multiplying the first of Eqs. (3.1) by σ and adding the second, multiplied by $Z+1$. Thus the function $V(\sigma, Z) := \sigma^2 + (Z+1)^2$ serves as a Lyapunov function for the dynamical system.

Let Γ denote the circle on which the right side of Eq. (3.10) vanishes, and let C_r denote the circle of radius r centered at $\sigma = 0$ and $Z = -1$; each C_r is a level set of V. The curves Γ and C_1 are shown in Fig. 5, which corresponds to the case of a single critical point, the spiral point C; and in Fig. 7, which corresponds to the case of three critical points. Notice that if $r > 1$, Γ lies strictly inside C_r. Consequently, Eq. (3.10) shows that the dynamical system flows inward at points along C_r. Thus the interior of C_r is an invariant set for each $r > 1$. Furthermore, the closed disk bounded by C_1, which is the intersection of these sets, is also invariant. For later convenience, denote by D the point where C_1 intersects the parabola on which $\dot{Z} = 0$.

We will also rely on some theorems for quadratic dynamical systems. The hypotheses for these theorems requires an analysis of the behavior of orbits at infinity, which is accomplished as follows. First, we introduce the variables $\rho > 0$ and $\varphi \in [0, 2\pi)$ such that $\sigma = \rho^{-1}\cos\varphi$ and $Z = \rho^{-1}\sin\varphi$. Thus $\rho = 0$ defines the circle at infinity. Second, we make a singular change of independent variable, from t to s, defined by $\rho\, ds = dt$, and we let a prime denote differentiation with respect to s. Then a simple calculation shows that

$$\begin{aligned} \rho' &= \left[1 + \varepsilon^{-1}\cos^2\varphi\right]\rho^2 + O(\rho^3)\,, \\ \varphi' &= \varepsilon^{-1}\cos\varphi + O(\rho)\,. \end{aligned} \tag{3.11}$$

Therefore the critical points at infinity ($\rho = 0$) occur at the angles $\varphi = \pm\pi/2$. Correspondingly, the eigenvalues in the angular direction are $\mp\varepsilon^{-1}$, while the eigenvalues in the radial direction vanish. Because the leading order term in ρ' is positive, the critical point at $\varphi = \pi/2$ is a saddle-node for which the separatrix leaves infinity, and the critical point at $\varphi = -\pi/2$ is a repelling node.

A.

Let us first consider the structure of the flow when there is a single critical point, located at C; see Fig. 5. As shown above, the point C must be an attracting spiral point. According to a theorem of Coppel [4], there is no periodic orbit for this quadratic dynamical system because the separatrix leaves the saddle-node at infinity. Thus the orbit through each point in the phase plane must spiral toward C.

In the application to the shear flow problem, we are interested in the particular solution of Eq. (3.1) with initial data $\sigma = 0$ and $Z = 0$ (point O). This solution initially remains inside the region $\mathcal{R}$ bounded by $ODVCO$ in Fig. 6, eventually exits through the arc CV of the parabola, and finally spirals toward C. Indeed, the orbit through O must remains inside C_1 and outside Γ because of Eq. (3.10); and for points along the portion of the parabola between D and V, $\dot{Z} = 0$ and $\dot{\sigma} < 0$, so that orbits cannot leave through DV. Therefore it must leave $\mathcal{R}$ along the arc CV of the parabola, whereupon it spirals into C. This solution is illustrated in Fig. 6.

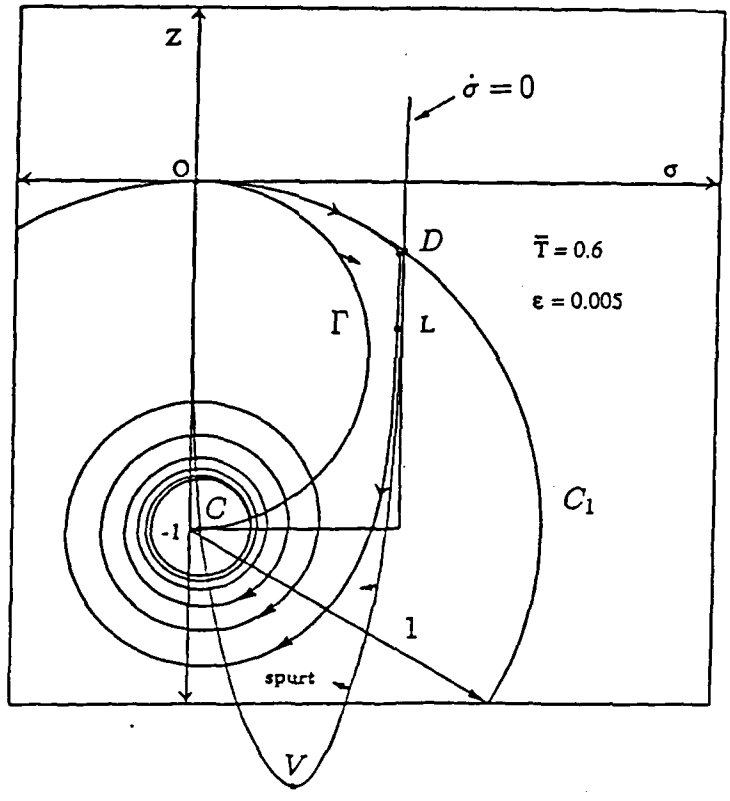

Fig. 6: The orbit through origin when the spurt attractor C is the only critical point.

B.

Next consider the case when there are three critical points, illustrated in Fig. 7. As shown by A. Coppel [private communication] using the Bendixson criterion, there are no periodic orbits or separatrix cycles for this quadratic dynamical system. Therefore, as t approaches infinity, the orbit through any point in the plane either: tends to A; tends to C; or tends to B along its stable manifold.

We first prove that the closed set $\mathcal{I}$ bounded by the curved triangle OAD is invariant with respect to Eqs. (3.1). To this end we show that orbits starting from points along OAD remain in $\mathcal{I}$. For points along C_1 strictly between O and D, this follows from the invariance of C_1. For points along the portion of the parabola between A and D (excepting A), $\dot{Z} = 0$ and $\dot{\sigma} < 0$, so that orbits lead into $\mathcal{I}$. Similarly, the flow leads into $\mathcal{I}$ along the arc of Γ strictly between A and O; this is because $\dot{Z} < 0$ and because of Eq. (3.10). Finally, A is a critical point, while the orbit through O must remains inside C_1 and outside Γ because of Eq. (3.10). One consequence of the invariance of $\mathcal{I}$ is that the solution of Eq. (3.1) with initial data $\sigma = 0$ and $Z = 0$ flows into the classical attractor A.

Next we study the stable manifold for the saddle point B in Fig. 7. Through this point we have drawn the circle C_B centered at $\sigma = 0$ and $Z = -1$, which intersects the parabola

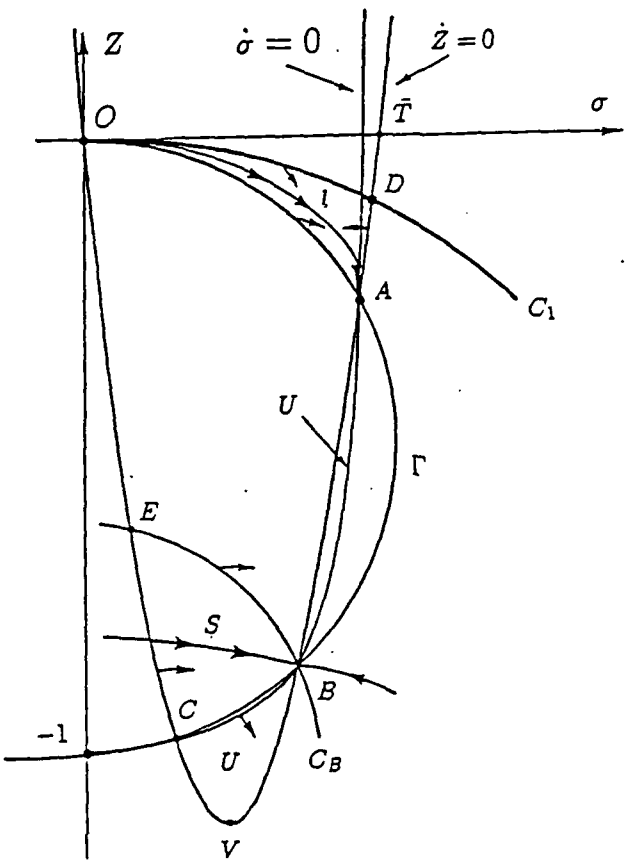

Fig. 7: Invariant regions in the case of three critical points.

at E. Let $\mathcal{S}$ denote the closed set bounded by the curved triangle ECB. At points on the boundary, the flow is directed as follows: outward from $\mathcal{S}$ along EB because of Eq. (3.10); outward along CB, where $\dot{Z} < 0$ and $\dot{V} = 0$; and inward along CE because $\dot{\sigma} > 0$ and $\dot{Z} = 0$. As a result, one branch of the stable manifold at B must enter $\mathcal{S}$ through the arc EC and remain is $\mathcal{S}$, as illustrated in Fig. 7. The other branch of the stable manifold enters B through the sector exterior to Γ and the circle C_B.

Notice that the basin of attraction of A, *i.e.*, the set of points that flow toward A as t approaches infinity, comprises those points on the same side of the stable manifold of B as is A; points on the other side are in the basin of attraction of C. For the purpose of analyzing the spurt phenomenon, we now show that the arc of Γ between B and the origin O is contained in the basin of attraction of A. This follows because the flow is directed into the region bounded by the following curves: Γ between B and A; the parabola between A and D; C_1 between D and O; the parabola between O and E; and C_B between E and B. Therefore this region is invariant. In particular, the stable manifold for B cannot cross the boundary, so that it cannot cross Γ between B and O.

Finally, consider the unstable manifold of the saddle point B. Let $\mathcal{U}_1$ be the set bounded by the arcs of the parabola $\dot{Z} = 0$ and the hyperbola $\dot{\sigma} = 0$ between the critical points B and A. Along the open arc of the parabola BA, $\dot{\sigma} > 0$, while along the open arc

of the hyperbola, $\dot{Z} > 0$. Therefore, one branch of the unstable manifold at B lies in $\mathcal{U}_1$ and connects B to A. Next consider the set $\mathcal{U}_2$ bounded by the arc BVC of the parabola $\dot{Z} = 0$ and the arc CB of the hyperbola $\dot{\sigma} = 0$. The flow is directed into $\mathcal{U}_2$ both along BV, where $\dot{\sigma} < 0$, and along CB, where $\dot{Z} < 0$. Therefore, the second branch of the unstable manifold at B remains in $\mathcal{U}_2$ until it exits through the arc VC. If C is a spiral point, this branch enters and leaves $\mathcal{U}_2$ infinitely often as it spirals into C, while if C is an attracting node, it does not reenter $\mathcal{U}_2$ as it tends to C.

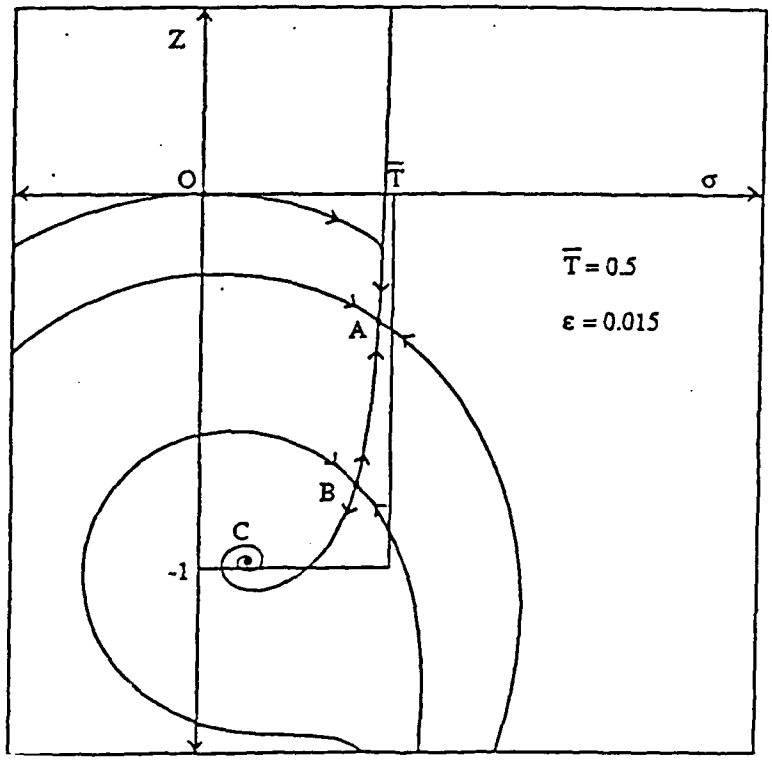

Fig. 8: Phase portrait in the case of three critical points, with C being a spiral.

To summarize the above description of the dynamics of the system (3.1) in the case of three critical points, with C being a spiral point, the reader is referred to Fig. 8.

C.

Finally consider the case of a single critical point at A, which is an attracting node. For quadratic dynamical systems, a periodic orbit must enclose a center or a spiral point [3]; thus there is no periodic orbit. As a result, all orbits are attracted to the node at A. The orbit through the origin remains in a region that is analogous to the region $\mathcal{I}$ in Fig. 7.

4. Features of the Mathematical Model in Relation to Experiment

The numerical simulations of (JS) described in Refs. [9, 13] exhibited several effects related to spurt: latency, shape memory, and hysteresis. For example, Fig. 9 shows the result of simulating a loading sequence in which the pressure gradient $\overline{f}$ is increased in small steps, allowing sufficient time between steps to achieve steady flow [9]. The loading sequence is followed by a similar unloading sequence, in which the driving pressure gradient is decreased in steps. The initial step used zero initial data, and succeeding steps used the results of the previous step as initial data. The resulting hysteresis loop includes the shape memory described in Ref. [7] for a simpler model. The width of the hysteresis loop at the bottom can be related directly to the molecular weight of the sample [9].

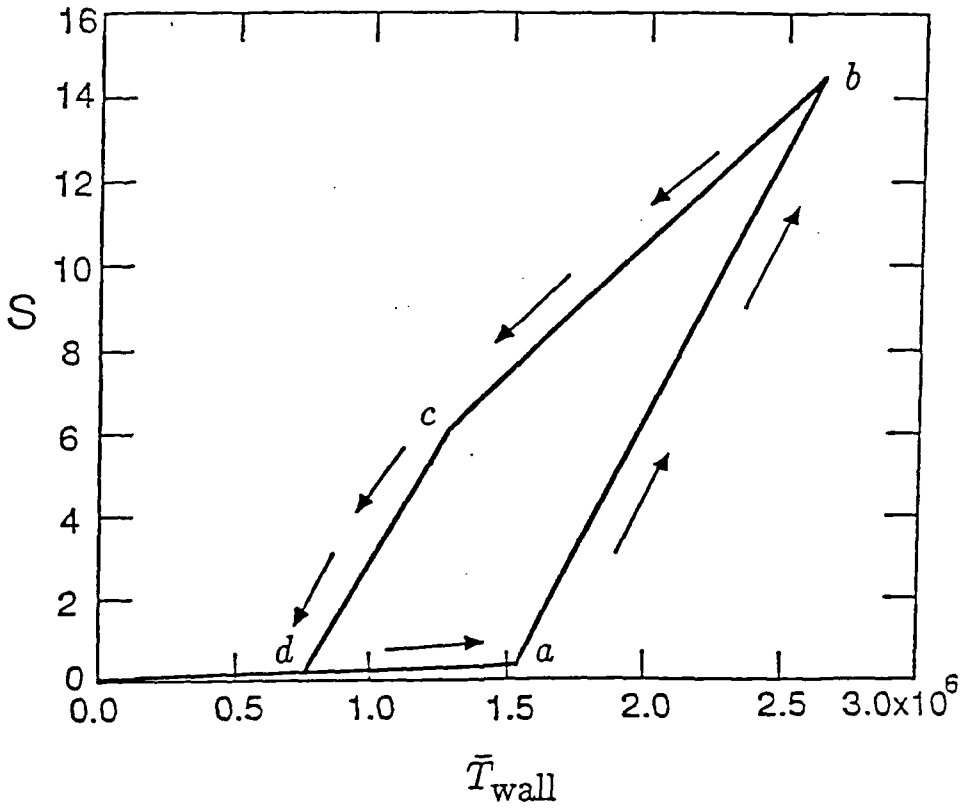

Fig. 9: Hysteresis under cyclic load: normalized throughput S *vs.* wall shear stress $\overline{T}_{\text{wall}}$ [9].

In this section we explain these effects using the results of the phase plane analysis of the dynamical system (3.1). We consider experiments of the following type: the flow is initially in a steady state corresponding to a forcing $\overline{f}$, and the forcing is suddenly changed to $\overline{f} + \Delta\overline{f}$. We call this process "loading" (resp. "unloading") if $\Delta\overline{f}$ has the same (resp. opposite) sign as $\overline{f}$.

Let us first establish some convenient terminology. Given a value of $\overline{f}$, the channel

$-1/2 \le x \le 0$ can be subdivided into three contiguous zones (subintervals) according to the size of $\overline{T}(x) = -\overline{f}x$. (Refer to Figs. 2 and 3.) We define Zone 1, which is nearest to the wall $x = -1/2$, to comprise those points x for which $\overline{T}(x) \ge \overline{T}_M$; this subinterval is nonempty if $\overline{f}$ is supercritical, *i.e.*, $\overline{f}/2 > \overline{T}_M$. For points in Zone 1, the only critical point of the system (3.1) is C, as in Fig. 5. In Zone 2, where $\overline{T}_m \le \overline{T}(x) \le \overline{T}_M$, there are three critical points, A, B, and C, as in Fig. 7; this subinterval is nonempty if $\overline{f}/2 > \overline{T}_m$. Zone 3, which is nearest to the centerline $x = 0$, consists of x for which $\overline{T}(x) \le \overline{T}_m$; the corresponding phase plane has only A as a critical point.

Notice also that the critical points for Eq. (3.1), with any value of $\overline{T}$, lie on the circle Γ, which is independent of $\overline{T}$. Let (σ_M, Z_M) denote the degenerate (double root) critical point that occurs when $\overline{T} = \overline{T}_M$, *i.e.*, at "top jumping" in Fig. 2; and let (σ_m, Z_m) denote the degenerate critical point for $\overline{T} = \overline{T}_m$, *i.e.*, for "bottom jumping." These points serve to divide Γ into arcs: Γ_A, the upper arc of Γ between (σ_M, Z_M) and $(-\sigma_M, Z_M)$; Γ_C, the lower arc between (σ_m, Z_m) and $(-\sigma_m, Z_m)$; and Γ_B, the remaining two arcs where $Z \in [Z_m, Z_M]$. For any value of $\overline{T}$, positive or negative, the classical attractor A lies in Γ_A, the spurt attractor C lies in Γ_C, and the saddle point B lies in Γ_B. Furthermore, as $|\overline{T}|$ is increased, the critical points A and C move downward along Γ, while B moves upward. This follows from Eq. (3.3) by differentiating the relation $Q(\sigma/\overline{T}) = 0$, to determine how $\sigma/\overline{T}$ varies with $\overline{T}$, and by using the first of Eqs. (3.2).

A. Startup

As a first experiment, consider starting from the quiescent state at the origin $\sigma = 0$, $Z = 0$ and loading to $\overline{f} > 0$. For each x in Zones 2 and 3 (near the centerline), the origin in the corresponding phase plane lies in the basin of attraction of the node at A, so that the orbit through the origin tends to A; this is illustrated in Fig. 8. For each x in Zone 1, by contrast, the origin is attracted to the sole critical point at C, as in Fig. 6. Accordingly, we draw two conclusions: (a) if $\overline{f}$ is subcritical, the flow approaches the classical solution corresponding to A at every point x; (b) if $\overline{f}$ is supercritical, the flow approaches a steady spurt solution in which the jump in strain rate occurs at the shear stress maximum $\overline{T}_M$ (which is top jumping in Fig. 2), *i.e.*, such that the kink in the velocity profile (see Fig. 3) is located as close as possible to the wall.

B. Loading

Next, consider increasing the load from a supercritical value $\overline{f} > 0$ to $\overline{f}_1 \ge \overline{f}$. This causes the three zones to shift: some points x previously in Zone 2 or 3 for $\overline{f}$ now lie in Zone 1 for $\overline{f}_1$. For each x in the new Zone 1, the corresponding phase plane for the system (3.1) has a unique critical point C_1, the spiral point. If such an x was previously in Zone 1 or 2, C_1 lies further down along Γ_C than was the corresponding attractor C for the smaller load $\overline{f}$. Similarly, for each x in the new Zone 2, there are three critical points, A_1, B_1, and C_1. Again, the spurt attractor C_1 lies further down along Γ_C, while the saddle point B_1 lies further up along Γ_B and the classical attractor A_1 lies further down along Γ_A, as compared to the corresponding critical points for $\overline{f}$. In particular, the stable manifold of B_1 lies above that of B, at least near to B_1. Finally, in the new Zone 3, there is a single critical point A_1 located downward along Γ_A with respect to A.

Let us now determine how the steady profile changes as a result of the increased load.

For every $x \in [-\frac{1}{2}, 0]$, we take the steady solution (σ_0, Z_0) attained at the load $\overline{f}$ as the initial point for an orbit in the phase portrait for the new load $\overline{f}_1$. If x belongs to the new Zone 1, the initial point (σ_0, Z_0) is either a classical attractor A, which disappeared as the loading was increased, or a spurt attractor C. Regardless, the orbit through this point leads to C_1 as time progresses because C_1 is the only critical point for the load $\overline{f}_1$. Thus spurt continues throughout the new Zone 1. By contrast, if x lies the new Zone 2 or 3, the initial point (σ_0, Z_0), which is a classical attractor A on Γ_A between A_1 and the origin, lies in the basin of attraction of the node A_1, and the corresponding orbit tends to A_1. To see this for points in Zone 2, notice that neither branch of the stable manifold of B_1 can intersect Γ between B_1 and the origin, as was shown in Sec. 3. Thus the domain of attraction of A_1, which is bounded by the stable manifold of B_1, contains A.

As a result, a point in x in the channel can change only from a classical attractor to a spurt attractor, and then only if $\overline{T}_1(x) = -\overline{f}_1 x$ exceeds $\overline{T}_M$. In other words, loading causes the position x_* of the kink in Fig. 3 to move away from the wall, but only to the extent that it must. (Formulas for the precise location are found in Refs. [9, 14].) Therefore, a loading process, without an intervening unloading, yields a jump in strain rate at total stress $\overline{T}_M$, *i.e.*, top jumping.

C. Latency

Our next task is to explain the latency effect that occurs during loading. In this context we assume that ε is small. It follows from Eqs. (2.5) and (2.6) that the total stress $\overline{T}_M$ at the the local maximum M is $1/2+O(\varepsilon)$, while the local minimum m corresponds to a total stress $\overline{T}_m$ of $2\sqrt{\epsilon}\,[1+O(\epsilon)]$. Furthermore, for x such that $\overline{T}(x) = O(1)$, $\sigma = \overline{T}+O(\varepsilon)$ at an attracting node at A, while $\sigma = O(\epsilon)$ at a spurt attractor C (which is a spiral). Consider a point along the channel for which $\overline{T}(x) > \overline{T}_M$, so that the only critical point of the system (3.1) is C, and suppose that that $\overline{T} < 1$. Then the evolution of the system exhibits three distinct phases, as indicated in Fig. 6: an initial "Newtonian" phase (O to N); an intermediate "latency" phase (N to S); and a final "spurt" phase (S to C).

The Newtonian phase occurs on a time scale of order ε, during which the system approximately follows an arc of a circle centered at $\sigma = 0$ and $Z = -1$. Having assumed that $\overline{T} < 1$, Z approaches

$$Z_N = (1 - \overline{T}^2)^{\frac{1}{2}} - 1 \tag{4.1}$$

as σ rises to the value $\overline{T}$. (If, on the other hand, $\overline{T} \geq 1$, the circular arc does not extend as far as $\overline{T}$, and σ never attains the value $\overline{T}$; rather, the system slowly spirals toward the spurt attractor. Thus the dynamical behavior does not exhibit distinct phases.)

The latency phase is characterized by having $\sigma = \overline{T}+O(\epsilon)$, so that σ is nearly constant and Z evolves approximately according to the differential equation

$$\dot{Z} = -\frac{\overline{T}^2}{Z+1} - Z\ . \tag{4.2}$$

Therefore, the shear stress and velocity profiles closely resemble those for a steady solution with no spurt, but the solution is not truly steady because the normal stress difference Z still changes. Integrating Eq. (4.2) from $Z = Z_N$ to $Z = -1$ determines the latency

period. This period becomes indefinitely long when the forcing decreases to its critical value; thus the persistence of the near-steady solution with no spurt can be very dramatic. The solution remains longest near point L where $Z = -1 + \overline{T}$. This point may be regarded as the remnant of the attracting node A and the saddle point B.

Eventually the solution enters the spurt phase and tends to the critical point C. Because C is an attracting spiral, the stress oscillates between the shear and normal components while it approaches the steady state.

D. Unloading: Shape Memory and Hysteresis

Now consider unloading from a steady solution for the load $\overline{f}_1$ to the load $\overline{f} < \overline{f}_1$; assume, for the moment, that $\overline{f}$ and $\overline{f}_1$ are both positive. The initial steady solution need not correspond to top jumping, as would be obtained by a pure loading process. Again the zones shift: some points previously in Zone 1 move into the new Zone 2 or 3. The orbit through any point in the new Zone 1 tends to the spurt attractor C for $\overline{f}$, and the orbit through any point in the new Zone 3 tends to the classical attractor A. More generally, the orbit through any point starting at a classical attractor A_1 leads to a new classical attractor A; this follows, as before, because the stable manifold for B cannot cross Γ between B and the origin. For points in the new Zone 2 that initiate at a spurt attractor C_1, however, there is an apparent choice of final rest state.

Clearly, the answer depends on whether C_1 lies on the same side of the stable manifold through B as does C. If this is true, the orbit through this point tends to C, so that spurt continues at this point. Suppose, for example, that it is true of all points in the new Zone 2 that initiate at a spurt attractor. Then all points that were classical remain classical, and spurt continues at all other points. Thus the position x_* of any jump in strain rate stays fixed, even though other flow characteristics (such as the magnitudes of the velocities) change. This phenomenon was termed "shape memory" by Hunter and Slemrod [7].

As an instance of this, suppose that the stress $\overline{T}(x)$ of smallest magnitude for points x in the spurt layer is strictly greater than $\overline{T}_m$. Then if $\overline{f}$ is sufficiently close to $\overline{f}_1$, $\overline{T}(x)$ for each x in the layer remains larger than $\overline{T}_m$; thus no point in the layer belongs to the new Zone 3. Moreover, for such an x, the stable manifold through B is only a slight perturbation of the stable manifold through B_1, which surrounds C_1, so that it surrounds C. Thus shape memory occurs in the situation where the stress in the layer is separated by a gap from $\overline{T}_m$ and the loading increment is sufficiently small. Because the stress at a jump in strain rate falls in the open interval $\overline{T}_m < \overline{T} < \overline{T}_M$, such solutions are referred to as "intermediate jumping;" this is the case illustrated in Fig. 2.

If, on the other hand, the minimum stress in the layer is $\overline{T}_m$ so that one layer boundary corresponds to bottom jumping, then the spurt layer must shift upon unloading. Indeed, there are points x in the layer for which $\overline{T}(x) < \overline{T}_m$, so that they have moved into the new Zone 3 and must flow to a classical attractor. The layer moves to the point x_* farthest from the wall such that $\overline{T}(x_*) = \overline{T}_m$. Similarly, shape memory is lost if $\overline{f}$ is lowered enough that $\overline{T}(x)$ drops below $\overline{T}_m$ in the layer. It is also possible, when the change in loading is large, for spurt attractors C_1 to lie on the opposite side of the stable manifold of B from C. This causes the formation of a region of classical flow next to the wall, which can coexist with intermediate spurt layers as well as the classical flow in the center of the channel.

This picture of shape memory explains the hysteresis loop in Fig. 9 obtained in a

loading–unloading sequence. In this figure, the throughput S, which is proportional to the area under the velocity profile in Fig. 3, is plotted as a function of the wall shear stress $\overline{T}_{\text{wall}} = \overline{f}/2$. The portion of this curve between the origin and a corresponds to subcritical loading, $\overline{T}_{\text{wall}} < \overline{T}_M$, while the segment ab corresponds to top jumping in supercritical loading. Unloading commences at b and continues along bc and cd. The throughput along bcd is different from the loading curve because intermediate and bottom jumping solutions occur along the unloading curve. In fact, the layer does not move during the process bc because of shape memory, so that the spurt layer is wider during unloading, resulting in larger throughput. At some point between b and c, the imposed $\overline{T}_{\text{wall}}$ becomes lower than $\overline{T}_M$; yet the flow remains supercritical. In such a situation, the flow would be subcritical at the corresponding stress in loading, and the difference in throughput in loading and unloading is particularly dramatic. At point c, bottom jumping commences, and the throughput decreases much more rapidly because the layer moves toward the wall. This accounts for the discontinuity in slope at c.

The salient features of this explanation of hysteresis are: the hysteresis loop opens from the point at which unloading commences; no part of the unloading path retraces the loading path until point d; and there is a discontinuity in slope of the unloading portion of the loop. These features stand in marked contrast to other plausible predictions of the nature of the hysteresis in spurt [15]; experiments are needed to verify which theory is correct.

E. Reloading and Flow Reversal

It is possible, of course, to apply more complex load sequences than those just described. For example, a loading sequence can be followed by unloading, which, in turn, is followed by reloading. Arguments extending the ones given above can be used to make qualitative predictions in such cases. For example, the layer position can remain fixed upon reloading.

Another striking phenomenon predicted by this analysis occurs when $\overline{f}_1$ and $\overline{f}$ have opposite signs and $|\overline{f}| < |\overline{f}_1|$. This more general form of unloading (defined in Ref. [9]) causes a reversal of the flow direction; surprisingly, though, the layer position can remain unchanged. For this to happen, the magnitude of the stress at the layer boundary must not fall below $\overline{T}_m$, and the stable manifolds of all saddle points B (which are now in the left half-plane of the phase portrait) must extend far enough into the right half-plane to enclose the spurt attractors C_1. For small ε, the stable manifold for a saddle point B is nearly a circle, and shape memory in flow reversal is more the rule than the exception. Because we doubted our observation of shape memory during flow reversals in numerical simulations, we were motivated to pursue the the more rigorous analysis described above.

F. Summary

To summarize, the phenomena of top jumping upon loading and shape memory and hysteresis upon unloading follow from analyzing the phase portraits of the approximating system (3.1). The analysis reduces to asking, for each point in the channel, whether or not the steady state for the initial load lies in the basin of attraction of the classical attractor for the new load. More complicated load sequences can be analyzed easily by answering this question.

5. Conclusions

The phase plane analysis of the approximating dynamical system (3.1) accurately reproduces the spurt behavior in viscoelastic shear flows that was observed experimentally by Vinogradov *et al.* [20] and numerically in Refs. [9, 12, 13]. Furthermore, this analysis predicts several associated phenomena, also observed numerically, such as latency, hysteresis, and shape memory; rheological experiments to verify these effects would be valuable.

Acknowledgments

We thank Professor A. Coppel for an elegant argument ruling out the existence of periodic and separatrix cycles for the system (3.1). We also acknowledge helpful discussions with D. Aronson, G. Sell, M. Slemrod and A. Tzavaras, and we thank M. Yao for help with the figures.

References

1. R. Bird, R. Armstrong, and O. Hassager, *Dynamics of Polymeric Liquids*, John Wiley and Sons, New York, 1987.

2. E. Coddington and N. Levinson, *Theory of Ordinary Differential Equations*, McGraw-Hill, New York, 1955.

3. A. Coppel, "A Survey of Quadratic Systems," *J. Differential Equations* **2** (1966), pp. 293–304.

4. A. Coppel, "A Simple Class of Quadratic Systems," *J. Differential Equations* **64** (1986), pp. 275–282.

5. M. Doi and S. Edwards, "Dynamics of Concentrated Polymer Systems," *J. Chem. Soc. Faraday* **74** (1978), pp. 1789–1832.

6. C. Guillopé and J.-C. Saut, "Global Existence and One-Dimensional Nonlinear Stability of ShearingMotions of Viscoelastic Fluids of Oldroyd Type," *Math. Mod. Numer. Anal.*, 1989. To appear.

7. J. Hunter and M. Slemrod, "Viscoelastic Fluid Flow Exhibiting Hysteretic Phase Changes," *Phys. Fluids* **26** (1983), pp. 2345–2351.

8. M. Johnson and D. Segalman, "A Model for Viscoelastic Fluid Behavior which Allows Non-Affine Deformation," *J. Non-Newtonian Fluid Mech.* **2** (1977), pp. 255–270.

9. R. Kolkka, D. Malkus, M. Hansen, G. Ierley, and R. Worthing, "Spurt Phenomena of the Johnson-Segalman Fluid and Related Models," *J. Non-Newtonian Fluid Mech.* **29** (1988), pp. 303–325.

10. R. Kolkka and G. Ierley, "Spurt Phenomena for the Giesekus Viscoelastic Liquid Model," F.R.O.G.-TR 88-20, Michigan Technical Univ., Houghton, MI, 1989.

11. Y.-H. Lin, "Explanation for Slip-Stick Melt Fracture in Terms of Molecular Dynamics in Polymer Melts," *J. Rheol.* **29** (1985), pp. 609–637.

12. D. Malkus, J. Nohel, and B. Plohr, "Time-Dependent Shear Flow of a Non-Newtonian Fluid," in *Current Progress in Hyperbolic Systems: Riemann Problems and Computations (Bowdoin, 1988)*, Contemporary Mathematics, ed. B. Lindquist, American Mathematics Society, Providence, RI, 1989. To appear.

13. D. Malkus, J. Nohel, and B. Plohr, "Dynamics of Shear Flow of a Non-Newtonian Fluid," *J. Comput. Phys.*, 1989. To appear.

14. D. Malkus, J. Nohel, and B. Plohr, "Phase-Plane and Asymptotic Analysis of Spurt Phenomena," in preparation, 1989.

15. T. McLeish and R. Ball, "A Molecular Approach to the Spurt Effect in Polymer Melt Flow," *J. Polymer Sci.* **24** (1986), pp. 1735–1745.

16. J. Nohel, R. Pego, and A. Tzavaras, "Stability of Discontinuous Shearing Motions of Non-Newtonian Fluids," in preparation, 1989.

17. J. Oldroyd, "Non-Newtonian Effects in Steady Motion of Some Idealized Elastico-Viscous Liquids," *Proc. Roy. Soc. London* **A 245** (1958), pp. 278–297.

18. B. Plohr, "Instabilities in Shear Flow of Viscoelastic Fluids with Fading Memory," in *Workshop on Partial Differential Equations and Continuum Models of Phase Transitions (Nice, 1988)*, ed. D. Serre, Springer–Verlag, New York, 1988. Lecture Notes in Mathematics, to appear.

19. M. Renardy, W. Hrusa, and J. Nohel, *Mathematical Problems in Viscoelasticity*, Pitman Monographs and Surveys in Pure and Applied Mathematics, Vol. 35, Longman Scientific & Technical, Essex, England, 1987.

20. G. Vinogradov, A. Malkin, Yu. Yanovskii, E. Borisenkova, B. Yarlykov, and G. Berezhnaya, "Viscoelastic Properties and Flow of Narrow Distribution Polybutadienes and Polyisoprenes," *J. Polymer Sci., Part A-2* **10** (1972), pp. 1061–1084.